A BENCHMARK BETWEEN HYMAGYC, MEGA AND ORB5 CODES USING THE NLED-AUG TEST CASE TO STUDY ALFVÉNIC MODES DRIVEN BY ENERGETIC PARTICLES

G. VLAD[1], X. WANG[2], F. VANNINI[2], S. BRIGUGLIO[1], N. CARLEVARO[1], M. FALESSI[1], G. FOGACCIA[1], V. FUSCO[1], F. ZONCA[1,3], A. BIANCALANI[2], A. BOTTINO[2], T. HAYWARD-SCHNEIDER[2], P. LAUBER[2]
[1]ENEA, Fusion and Nuclear Safety Department, C. R. Frascati, Via E. Fermi 45, 00044 Frascati (Roma), Italy
[2]Max-Planck-Institut für Plasmaphysik, Boltzmannstr. 2, 85748 Garching, Germany
[3]Institute for Fusion Theory and Simulation and Department of Physics, Zhejiang University, Hangzhou 310027, People's Republic of China
e-mail contact of main author: gregorio.vlad@enea.it

Abstract

One of the major challenges in magnetic confinement thermonuclear fusion research concerns the confinement of the energetic particles (EPs) produced by fusion reactions and/or by additional heating systems. In such experiments, EPs, having their velocities of the order of the Alfvén velocity, can resonantly interact with the shear Alfvén waves. In order to predict and, eventually, minimize the Energetic Particle (EP) transport in the next generation fusion devices, several numerical models, based on different theoretical approaches, have been developed. For this purpose, in the frame of the EUROfusion 2019-2020 Enabling Research project "Multi-scale Energetic particle Transport in fusion devices" (MET), a detailed benchmark activity has been undertaken among few of the state-of-the-art codes available to study the self-consistent interaction of an EP population with the shear Alfvén waves, in real magnetic equilibria and in regimes of interest for the forthcoming generation devices (e.g., ITER, JT-60SA, DTT). The codes considered are HYMAGYC, MEGA, and ORB5, the first two being hybrid MHD-Gyrokinetic codes (bulk plasma is represented by MHD equations, while the EP species is treated using the gyrokinetic formalism), the third being a global electromagnetic gyrokinetic code. The so-called NLED-AUG reference case has been considered, both for the peaked on-axis and peaked off-axis EP density profile cases, using its shaped cross section version. This reference case poses an exceptional challenge to the codes due to its high EP pressure, the rich spectrum of experimentally observed instabilities and their non-linear interaction. Perturbations with toroidal mode number $n = 1$ will be considered. Comparison of the spatial mode structure, growth rate and real frequency of the modes observed will be considered in detail. Dependence of mode characteristics as several parameters are varied, as, e.g., the ratio between EP and bulk ion density and energetic particle temperature, will be presented.

1. INTRODUCTION

One of the major challenges in magnetic confinement thermonuclear fusion research concerns the confinement, inside the reaction chamber, of the Energetic Particles (EPs) produced by fusion reactions and/or by additional heating systems, as, e.g., electron and ion cyclotron resonant heating, and neutral beam injection. In such experiments, EPs, having their velocities of the order of the Alfvén velocity, can resonantly interact with the shear Alfvén waves. In order to predict and, eventually, minimize the EP transport in the next generation fusion devices, several numerical models, based on different theoretical approaches, have been developed. In this respect, it is crucial to cross verify and validate the different numerical instruments available in the fusion community. For this purpose, in the frame of the EUROfusion 2019-2020 Enabling Research project "Multi-scale Energetic particle Transport in fusion devices" (MET) [1], a detailed benchmark activity has been undertaken among few of the state-of-the-art codes available to study the self-consistent interaction of an EP population with the shear Alfvén waves, in real magnetic equilibria and in regimes of interest for the forthcoming generation devices (e.g., ITER [2], JT-60SA [3], DTT [4]). The codes considered in this benchmark are HYMAGYC [5], MEGA [6], and ORB5 [7], the first two being hybrid MHD-Gyrokinetic codes (bulk plasma is represented by MHD equations, while the EP species is treated using the gyrokinetic formalism), the third being a global electromagnetic gyrokinetic code (both bulk and EP species are treated using the gyrokinetic formalism). The so-called NLED-AUG [8] reference case has been considered, both for the peaked on-axis and peaked off-axis EP density profile cases, using its shaped cross section version. This test case poses an exceptional challenge to the codes due to its high EP pressure, the rich spectrum of experimentally observed instabilities and their non-linear interaction [9].

Particular care has been devoted to consider plasma and numerical parameters as close as possible among the three codes: the same input equilibrium file (EQDSK) has been considered, ion density profile has been obtained by imposing quasi-neutrality ($Z_in_i+Z_Hn_H = n_e$), as required by ORB5 (here n_i, n_e, n_H are the bulk ions, electrons, and EP densities (both bulk ion and EPs are assumed to be Deuterons), respectively, and Z_i, Z_H their electric charge numbers); finite resistivity and adiabatic index $\Gamma = 5/3$ have been assumed for both the hybrid codes (this is the usual choice used in MEGA, where also some viscosity is considered to help numerical convergence). Only finite orbit width (FOW) effects have been retained in this benchmark, and an isotropic Maxwellian EP distribution function of Deuterons with T_H=0.093 MeV, constant in radius, has been considered. Perturbations with single toroidal mode number $n = 1$ will be considered; the results of simulations considering both off-axis and on-axis peaked EP density profiles will be presented.

The paper is organized as follows: in Sec. 2 a brief description of the codes participating to this benchmark will be given, as well as the setting up of the benchmark equilibrium and the specific code parameters used; in Sec. 3 a characterization of the equilibrium in the MHD limit will be presented; in Sec. 4 the results of linear simulations will be presented for the nominal cases in Sec. 4.1, for the results of scanning the EP density in Sec. 4.2, as well as for the results of scanning the EP temperature in Sec. 4.3; in Sec. 5 some concluding remarks will be presented.

2. CODES, EQUILIBRIUM AND NUMERICAL PARAMETERS

As anticipated in the Introduction, three codes has been considered for this benchmark: HYMAGYC [5], MEGA [6], and ORB5 [7]. The HYMAGYC code [5] is a Hybrid Magnetohydrodynamics Gyrokinetic Code suitable to study EP driven Alfvénic modes in general high-β axisymmetric equilibria, (with β being the ratio of the plasma pressure to the magnetic pressure), with perturbed electromagnetic fields (electrostatic potential φ and vector potential $\mathbf{A}$) fully accounted for. The thermal plasma is described by linear, full, resistive MHD equations in arbitrary axis-symmetric equilibria. The MHD field solver relies on equilibrium quantities computed by the equilibrium code CHEASE [10] (as, e.g., covariant and contravariant components of the metric tensor coefficients, Jacobian, equilibrium magnetic field, current density components and pressure); it is also fully interfaced with the European Integrated Modelling Framework data structure [11] (formerly ITM, presently maintained by the EU-IM Team[1]) and the IMAS environment [12]. Such field solver originates from the code MARS [13], which has been transformed from an eigenvalue solver to an initial value one (see Appendix A.2 in [14]) which uses a fully implicit (backward Euler) finite difference time discretization scheme. The MARS kernel uses Fourier decomposition in generalized poloidal (χ) and toroidal (ϕ) angles and generalized finite element method along with the Tunable Integration Method [15] for the discretization in the radial-like coordinate $s = \sqrt{|\psi - \psi_0|/|\psi_{edge} - \psi_0|}$ (with ψ the equilibrium poloidal flux function, and ψ_0 and ψ_{edge}, respectively, the value of ψ on the magnetic axis and at the last closed magnetic surface). The EP population is described by the nonlinear gyrokinetic Vlasov equation, solved by particle-in-cell (PIC) techniques, and expanded up to order O(ϵ^2) and O($\epsilon\epsilon_B$), ϵ being the gyrokinetic ordering parameter $\epsilon \sim \rho_H/L_n$ and $\epsilon_B \sim \rho_H/L_B$, with ρ_H the energetic ("Hot") particle Larmor radius, L_n and L_B the characteristic equilibrium plasma density and magnetic-field nonuniformity length scales, respectively. As $L_n/L_B \ll 1$, O(ϵ_B^2) terms are neglected. The perturbed electromagnetic fields are assumed to be low-frequency fluctuations characterized by short wavelengths perpendicular to the equilibrium magnetic field and long wavelengths parallel to it. The following space-time ordering for the fluctuating electromagnetic fields holds [16]: $k_\perp\rho_H = O(1)$, $k_\parallel\rho_H = O(\epsilon)$, $\omega/\Omega_H = O(\epsilon)$, being $k_\perp$ the perpendicular (to the equilibrium magnetic field) wave vector of perturbed fields, $k_\parallel$ the parallel one, ω the characteristic fluctuation frequency and $\Omega_H = q_HB/m_Hc$ the EP gyrofrequency, with q_H, m_H, B and c the EP charge and mass, the equilibrium magnetic field and the light velocity, respectively. Flux coordinate system (s, χ, ϕ) is used. The MHD solver can consider finite resistivity η and finite adiabatic index Γ, but no viscosity. The coupling between MHD and EPs is obtained by adding to the MHD momentum equation a term proportional to $\nabla \cdot \Pi_k$ [17] (Π_k being the EP stress tensor).

In the MEGA code [6], the bulk plasma is described using nonlinear full MHD equations, and the EPs are described by the drift-kinetic equation. The energetic ion contribution is included in the MHD momentum equation as the EP current density j'_H that includes the contributions from parallel velocity, magnetic curvature and gradient drifts, and magnetization current. The $E\times B$ drift disappears in j'_H owing to quasi-neutrality. The electromagnetic field is given by the standard MHD description, as well as by the Hazeltine and Meiss equations [18]. The MHD equations are solved using a finite-difference scheme of fourth-order accuracy in space and time. Resistivity, viscosity and diffusion terms are included in the equations. Moreover, and adiabatic index $\Gamma = 5/3$ is also used in the MHD solver. Note that (R, ϕ, Z) coordinates are used for solving the equations, while flux coordinates are considered for the result analysis. In the present paper only standard MHD description will be considered.

ORB5 [7] is a global, nonlinear, electromagnetic, particle-in-cell code which solves the gyrokinetic Vlasov-

[1] See http://www.euro-fusionscipub.org/eu-im

Maxwell system of equations described in Refs. [19, 20]. It can take into accounts collisions and heat, particle and momentum sources (which are neglected in the present work). The distribution function of each species "sp" is composed by a time-independent background component $F_{0,sp}$ and a time-dependent part δf_{sp}. The latter is represented by sample of numerical particles (markers), which are pushed with a 4th-order Runge-Kutta scheme along the trajectories defined by the equation of motion of the gyrocenter characteristics $(\boldsymbol{R}, v_\parallel, \mu)$. In ORB5 straight field-line coordinates are used: (s, θ^*, ϕ). The radial coordinate $s = \sqrt{\psi/\psi_0}$ is provided in term of poloidal flux ψ normalized at its value at the edge ψ_0. The angular coordinates are the torodial angle ϕ and the poloidal magnetic angle $\theta^* = q^{-1}(s)\int_0^\theta [(\boldsymbol{B}\cdot\nabla\phi)/(\boldsymbol{B}\cdot\nabla\theta')]d\theta'$, where $q(s)$ is the safety factor profile and θ the geometric poloidal angle. The equations of motion are coupled with the field equations: the Poisson equation (in the quasi-neutrality limit) and the parallel Ampère's law. These are solved using finite elements (typically cubic B-splines) on a grid $(N_s, N_{\theta^*}, N_\phi)$. A field-aligned Fourier filter is used [21]. At each radial grid point s, for each toroidal mode n, only the poloidal modes $m \in [-n \cdot q(s) \pm \Delta m]$ are retained, being Δm the width of the retained poloidal modes. The equations are solved through a mixed-variable pullback algorithm in order to mitigate the so-called cancellation problem [22].

For the purpose of this benchmark, all the codes will consider only Finite Orbit Width (FOW) effects, neglecting Finite Larmor radius (FLR) ones.

The equilibrium chosen for this benchmark is a "variant" of the AUG test case, originally proposed by Ph. Lauber within the EUROfusion Enabling Research NLED [8]: the AUG shot considered is the #31213, at t=0.84s. In order to use such test case to execute this benchmark on a realistic, fully shaped equilibrium, we have considered the fully shaped cross section version of this equilibrium [8], as described by a standard EQDSK file (see Fig. *1.*). The equilibrium, as defined in the original AUG EQDSK file, has been scaled using the equilibrium code CHEASE [10] in order to keep exactly the on-axis safety factor q_0 as tabulated in the EQDSK file itself, namely $q_0 \simeq 2.39897$: this choice results in a toroidal Alfvén gap fully open, when considering the reference bulk mass plasma density profile. Also, the experimental equilibrium has been transformed such to have both positive toroidal magnetic field and plasma current, when considering the coordinate system (R, Z, ϕ) used by CHEASE [10], and (s, χ, ϕ) used by HYMAGYC (also described by the so-called COCOS number, COCOS=2 [23]). As a final remark, the plasma boundary has been slightly smoothed, in order to remove the sharpness of the experimental AUG X-point (both CHEASE and HYMAGYC assume closed magnetic surface domain). As a result of these approximations, a new EQDSK file has been shared among the different codes for the benchmark exercise, being characterized by on-axis toroidal magnetic field $B_0 \simeq 2.208$ [T], on-axis major radius $R_0 \simeq 1.666$ [m], plasma current $I_p \simeq 8.1434 \times 10^5$ [A], inverse aspect ratio $\epsilon_0 \simeq 0.297898$.

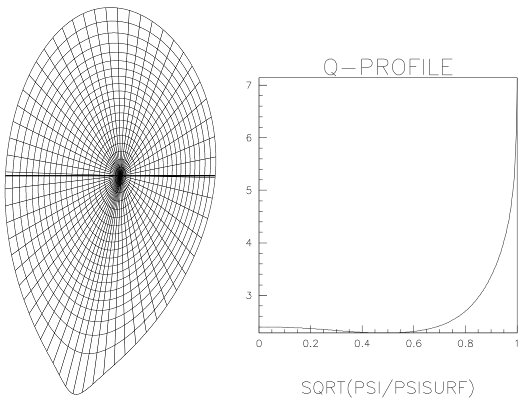

FIG. 1.: Poloidal cross section (left) and safety factor profile q (right) as function of the square root of the normalized poloidal flux for the considered NLED-AUG test case.

Electron and energetic particle (Deuterium) density profiles are shown in Fig. *2.*, as given by the original AUG NLED case [8]: two variants for the EP density profile are considered, the peaked on-axis EP density profile (see Fig. *2.*, red, long-dashed curves), and the peaked off-axis one (see Fig. *2.*, blue, short-dashed curves), with the Deuterium bulk-ion density profiles defined, for both cases, as $Z_i n_i(s) = n_e(s) - Z_H n_H(s)$ (here n_i, n_e, n_H are the bulk ions, electrons, and EP densities (both bulk ion and EPs are assumed to be Deuterons), respectively, and $Z_i = Z_H = 1$ their electric charge numbers). Maxwellian distribution function will be assumed for the EPs with a constant in radius temperature profile $T_H(s) = 0.093$ [MeV]. Although not strictly required, hybrid codes, as MEGA and HYMAGYC, usually consider some kind of diffusivity, for helping the numerics: the MHD solver of MEGA considers both resistivity η and viscosity ν, while the MHD solver of HYMAGYC considers only resistivity. Within the simulations of the present benchmark, normalized resistivity given in terms of the inverse Lundquist number $S^{-1}_{\mathrm{MEGA}} = 5 \times 10^{-7}$ will be used (here, $S_{\mathrm{MEGA}} \equiv \mu_0 R_0 (v_{A0}/\eta)$,

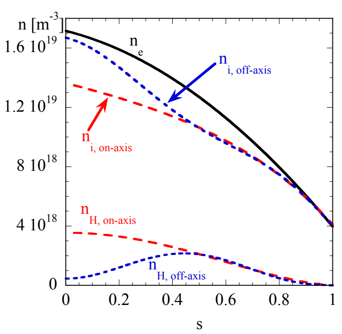

FIG. 2.: Ion densities for the peaked on-axis (red, long-dashed curves), and off-axis (blue, short-dashed curves) EP profiles. Electron density is shown in black, solid curve.

with v_{A0} the on-axis Alfvén velocity; note that the definition of the normalized resistivity in HYMAGYC differs from the one of MEGA, being $S_{\text{HYMAGYC}} \equiv \mu_0(a^2/R_0)(v_{A0}/\eta))$. A similar value for the normalized viscosity is used in MEGA, being $\nu_{\text{norm}} \equiv \nu/(R_0 v_{A0}) = 5 \times 10^{-7}$. Both HYMAGYC and MEGA use, for the adiabatic index, the value $\Gamma = 5/3$ (note that finite values of Γ allows for both shear Alfvén and acoustic branches of the Alfvén continuous spectra).

The HYMAGYC MHD solver (which is derived from the full linear, resistive, MHD solver MARS [13]) solves the MHD equations in flux coordinates (s, χ, ϕ) after expanding in Fourier components in the angular coordinates (χ, ϕ) and using finite elements in s (being $s = 0$ on the magnetic axis and $s = 1$ on the plasma boundary). The equilibrium quantities are provided by CHEASE, which solves the Grad-Shafranov equation and maps the solution to the considered flux-coordinate system. In CHEASE, the Jacobian of the transformation from the flux coordinates (s, χ, ϕ) to the Cartesian coordinates is restricted to the form $J = C(s)R^{\alpha}|\nabla\psi|^{\mu}$, with α and μ integers, R the major radius and ψ the poloidal magnetic flux function, and $C(s)$ being obtained by imposing periodicity after a poloidal turn. In the following simulations of HYMAGYC, a χ angle defined by the Jacobian $J \propto R/|\nabla\psi|$ (i.e., $\alpha = 1$, $\mu = -1$, the so-called *equal arc length* coordinate system) will be considered: such a choice of the poloidal angle-like variable χ usually minimizes the number of Fourier components required to obtain a well converged solution.

Specific code parameters used throughout this benchmark are as follows: HYMAGYC will use, for the field solver module, a radial (s) mesh of 180 equally spaced grid points, and a poloidal Fourier spectrum $m = [-3, 13]$, for the considered $n = -1$ toroidal mode; note, however, that the condition of purely real perturbation in the configuration space imposes always to consider a symmetric spectrum of perturbation in the Fourier space (m, n), such that $f_{\text{m,n}} = f^*_{-\text{m},-\text{n}}$, f being a generic perturbed field. Regarding the gyrokinetic module, the numerical markers describing the EP distribution function will be evolved in a 3D flux coordinates space (s, χ, ϕ) using $180 \times 120 \times 8$ grid points, and, typically, a number of simulation particles per cell $N_{\text{part/cell}} = 64$, thus considering a total number of EP markers $N_{part} = 11,059,200$. The number of grid points used for MEGA simulations for the cylindrical coordinates (R, ϕ, Z) is $128 \times 16 \times 256$. The number of marker particles used is 8,388,608, i.e., $N_{\text{part/cell}} = 16$. The output of MEGA is in flux coordinates space (s, ϕ, θ), and the Fourier components are chosen by n=[-1,0,1] and m=[0,64]. The number of grid points for ORB5 simulations for the coordinate system (s, θ^*, ϕ) is $2000 \times 144 \times 48$ and the number of markers M, respectively, for bulk ions, EPs, and electrons are $M_i = M_{EPs} = 3 \times 10^7$, and $M_e = 12 \times 10^7$. Other typical parameters tor the two scenarios considered (AUG peaked on-axis, and AUG peaked off-axis EP density profiles) are: n_{e0} = 0.171587 [$10^{20}/m^3$], n_{H0} = (0.03552, 0.00458182) [$10^{20}/m^3$], n_{i0} = (0.136067, 0.16700518) [$10^{20}/m^3$] being, respectively, the on-axis electron, energetic particles and bulk ion densities, ω_{A0} = (5.53876 $\times$ 10^6, 4.99947 $\times$ 10^6) [rad/s] the on-axis Alfvén frequency, $v_{H,th0}$ = 2.1111 $\times$ 10^6 [m/s] the on-axis EP thermal velocity, ρ_{H0} = 0.0199221 [m] the on-axis EP Larmor radius, thus giving, for the adimensional characteristic parameters, n_{H0}/n_{i0} = (0.261048, 0.0274352), $v_{H,th0}/v_{A0}$ = (0.228782, 0.253461), ρ_{H0}/a = 0.041279.

3. CHARACTERIZATION OF ALFVÉNIC SPECTRA OF OSCILLATIONS IN THE MHD LIMIT

In order to characterize the equilibrium described in Sec. 2 with reference to the MHD frequency spectra (continuous oscillations and global modes), we have run the hybrid MHD-gyrokinetic codes HYMAGYC and MEGA using the reference on-axis EP density profile but neglecting the EP contribution (i.e., switching off the coupling terms between gyrokinetic and fluid equations and searching for purely MHD solutions), by assigning an arbitrary initial condition and let evolving it in time. In absence of a EP drive terms, the perturbed equilibrium is fully stable, apart from a weakly growing mode which can be identified as a tearing mode (see later). In order to analyze and identify the different type of oscillations admitted by this equilibrium, it is instructive to

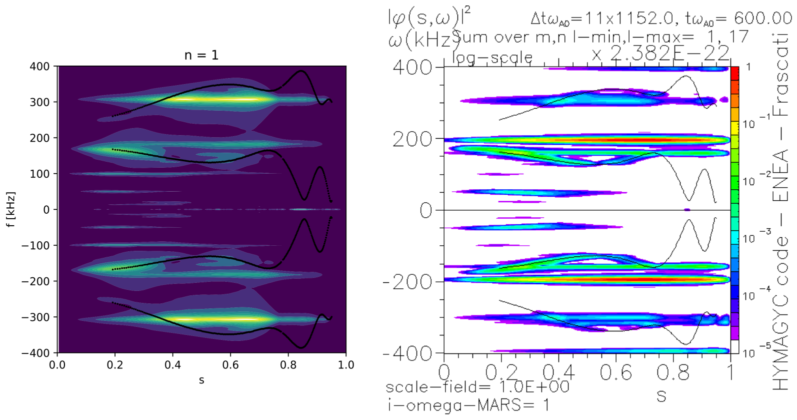

FIG. 3.: Frequency spectra in the MHD limit for MEGA (left) and HYMAGYC (right). Logarithmic color scale is used for the intensity of the e.s. field $|\varphi(s,\omega)|^2$. Shear Alfvén coutinuous spectra are also shown using black continuous lines.

Fourier analyze in time the results of the simulations, as shown in Fig. *3.*, where the frequency spectra $|\varphi(s,\omega)|^2$ of the electrostatic field $\varphi_{\rm m,n}(s,t)$ are illustrated for MEGA and HYMAGYC. In Fig. *3.* also the shear Alfvén continuous spectra are shown for reference (plotted using black continuous lines), as obtained by the FALCON code [24] in the limit of slow-sound approximation [25] (acoustic Alfvén continua as obtained by FALCON, although present in the system, are not shown for the sake of clarity of the figures). The frequency spectrum is almost perfectly symmetric w.r.t. the ω sign. A variety of oscillations are observed, almost all of them being damped (apart from a weakly growing mode). We will refer, in the following, to lower and upper shear Alfvén continuous spectra as the ones with lower and higher values of *absolute* frequencies, respectively.

To better enlighten the different global modes and local oscillations observed in the simulations, a logarithmic color scale representing the amplitude of the power spectra has been used. Both MEGA and HYMAGYC clearly show few dominant global (radially extended) modes localized in frequency within the toroidal Alfvén gap (TAEs), few modes localized below the lower shear Alfvén continuous spectrum, which could belong to the β induced branch (BAE), and (only HYMAGYC) a mode lying above the upper toroidal Alfvén continuous spectrum, within the ellipticity Alfvén gap (EAE). Also a clear evidence of local oscillations superimposed to the lower toroidal Alfvén continuous spectrum are observed, showing that both codes well represent the continua oscillations. In order to be able to compute damping- (and growth-) rates, it is worthwhile to perform frequency Fourier spectra using a “time window” shorter that the full simulation duration, and track in time the amplitudes variation of the frequency spectra obtained in that way. Using such analysis (which is routinely done on the HYMAGYC simulations), one can, e.g., track the relative maxima of the frequency spectra, together with their localization in frequency and radial-like coordinate, and identify the different characteristics of the oscillations observed (ω, γ, nature of the modes, etc.): this is shown in Table I. Note that also a weakly growing mode is reported for the simulation of HYMAGYC, which is radially localized at $s \approx 0.85$, at the radial position were $q(s) = 3$, thus being identified as a tearing mode ($m = 3, n = -1$). In Table I also few modes identified in a similar simulation by ORB5 are shown, in quite good agreement with the two hybrid codes of this benchmark, namely, HYMAGYC and MEGA; the only difference w.r.t. the hybrid codes being that the bulk ion profile for the ORB5 simulation must be $n_i = n_e$, quasi-neutrality being mandatory for fully gyrokinetic codes, and the different bulk ion density profile reflecting, as a consequence, in a slightly different shear Alfvén frequency spectra.

$\gamma_{\rm HYMAGYC}$ $[s^{-1}]$	$\omega_{\rm HYMAGYC}$ [kHz]	$\gamma_{\rm MEGA}$ $[s^{-1}]$	$\omega_{\rm MEGA}$ [kHz]	$\gamma^{\dagger}_{\rm ORB5}$ $[s^{-1}]$	$\omega^{\dagger}_{\rm ORB5}$ [kHz]
4080.2	0.0				
-9267.0	-49.3				
-14594.6	-159.2	-45060.0	-171.9	$\approx -10000.$	-146.
-6455.3	-195.8	-36057.0	-185.2	$\approx -6000.$	-206.
-29484.2	-301.4	-30120.0	-304.2		
-13542.3	-395.8				

TABLE *I: Growth rates $[s^{-1}]$ and real frequencies [kHz] of some of the modes observed in Fig. 3., corresponding to the HYMAGYC, MEGA and ORB5 purely MHD simulations, on-axis AUG reference case. (†) Note that for the ORB5 simulation, $n_i = n_e$ has been considered, whereas both HYMAGYC and MEGA assume $n_i = n_e - n_{H,\rm on-axis}$, with $n_{H,\rm on-axis}$ the peaked on-axis EP density, while neglecting the EP contribution in the fluid equations.*

4. LINEAR RESULTS OF THE BENCHMARK

In this Section we present the linear stability results obtained by the three codes, comparing the radial structure of the most unstable modes observed in the simulations and their frequency power spectra of both the peaked on-axis and off-axis EP density profiles. In particular, the results of simulations for the nominal values will first be shown in Sec. 4.1, and lately the analysis of the simulation results with the dependence on the intensity of the drive when varying, separately, the EP density (see Sec. 4.2) and EP temperature (see Sec. 4.3) will be presented.

4.1. NOMINAL CASES COMPARISON

In Fig. *4.* the results of the three codes for the two reference cases are shown: in both cases, for all the three codes considered, a mode driven by the EP is observed. Let’s consider, first, the results for the peaked on-axis EP density profile (Fig. *4.*, left column): after an initial transient phase of the simulations, both HYMAGYC and MEGA observe, as the most unstable, a mode located around $s \approx 0.4$, with a dominant $m = 2$ poloidal Fourier component for the electrostatic field φ, and located around $\omega \approx -130$ kHz in frequency, i.e., with a frequency slightly lower (in absolute value) than the lower shear Alfvén continuous spectrum: these observations, together with the fact that its radial location is quite close to the minimum q value (see Fig. *1.*, right), suggest that this mode is a so-called Reversed Shear Alfvén Eigenmode (RSAE). On the other side, the results of ORB5 show, for the most unstable mode, a more externally localized structure ($s \approx 0.7$) dominated by $m = 2, 3$, and localized, in frequency, close to the lower (in absolute value) tip of the toroidal gap throat, $\omega \approx -200$ kHz. When considering the peaked off-axis EP density profile, on the other side (Fig. *4.*, right column), all the three codes show a very good agreement. In particular, all of them observe a mode located, radially, close to the magnetic axis ($s \approx 0.2$), dominated by a $m = 2$ poloidal Fourier component, and located, in frequency, within the toroidal gap and with opposite sign w.r.t. to the previous, peaked on-axis, case. Note that the radial localization correspond to the EP density profile characterized by a positive radial gradient (see Fig. *2.*), i.e., with opposite sign w.r.t. to the peaked on-axis, monotonically decreasing, EP density profile (and, thus, with opposite sign of the diamagnetic frequency of the EPs driving term $\propto \omega_H^*$ [26]). Some more insight on the results of the simulations, and, in particular,

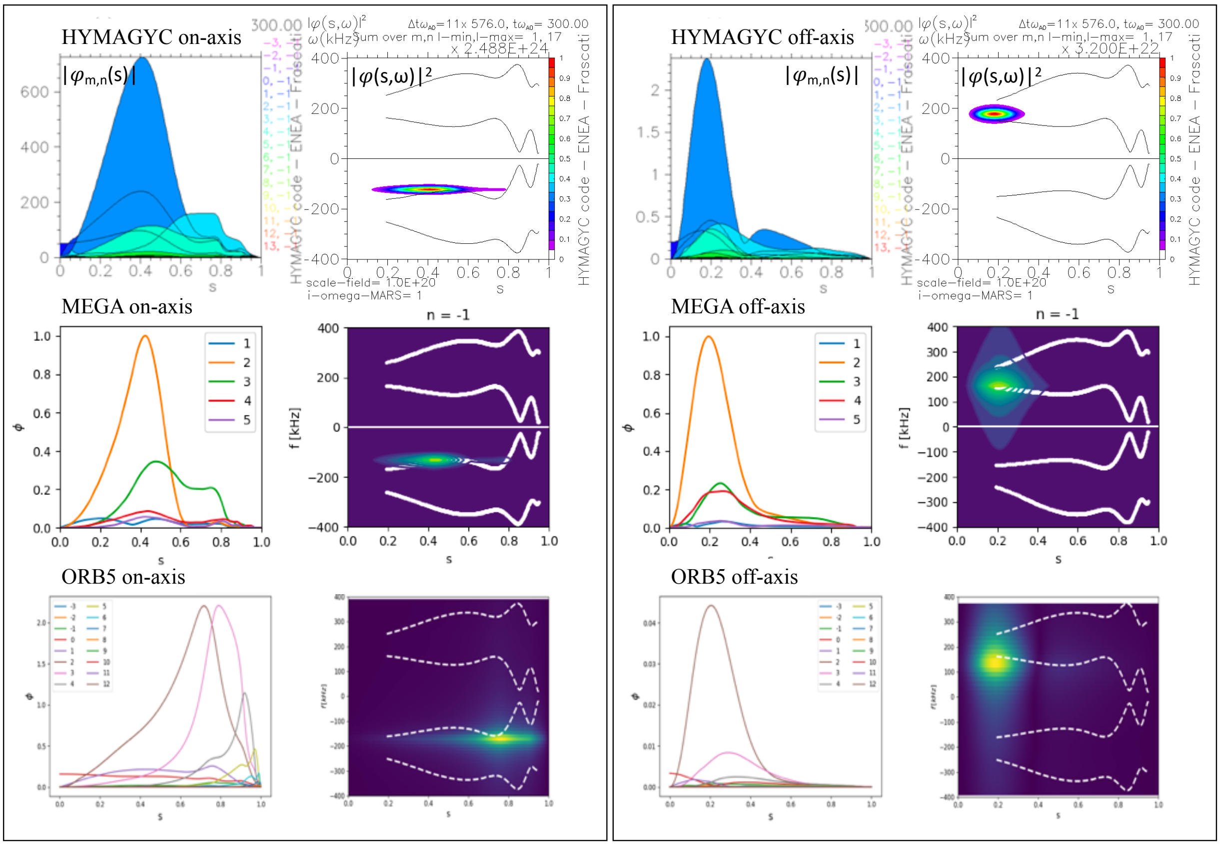

FIG. 4.: Comparison between the results obtained for HYMGYC (top row), MEGA (centre row), ORB5 (bottom row), for the two AUG nominal cases: peaked on-axis EP density profile (left column) $n_{H0}/n_{i0} = 0.261$, $T_H = 0.093$ MeV, and peaked off-axis EP density profile (right column) $n_{H0}/n_{i0} = 0.0274$, $T_H = 0.093$ MeV. The radial profiles for different poloidal Fourier components of the e.s. potential $\varphi(s)$, and its power frequency spectra are plotted for each case (linear color scale).

regarding the discrepancies observed, for the peaked on-axis EP density profile case, among ORB5 on one side, and HYMAGYC and MEGA on the other side, can be gained by comparing the results of the simulations performed by varying two parameters, namely, the on-axis EP density n_{H0} and temperature T_{H0}, as will be shown in the next sub-Sections 4.2 and 4.3.

4.2. ENERGETIC PARTICLE DENSITY SCAN

In this Section we present the results of varying the EP density w.r.t. the reference case values. We will focus our attention to the growth rate of the mode observed in the simulations, and, possibly, connect the results to the one presented in the so-called MHD limit presented in Sec. 3. Indeed, varying the EP density will modify, accordingly, the intensity of the EP drive, while keeping unchanged the EP motion, i.e., their resonances and characteristic frequencies. Note that, in order to correctly satisfy the quasi-neutrality requirement of ORB5, the bulk ion density profile will be recomputed accordingly: this imply, as a consequence, that the ω_{A0} value and Alfvén shear continua will slightly change for each different value of n_{H0} considered in the simulations. Figure *5.* shows the results of the EP density scan for the on-axis EP density profile, ranging from the MHD limit ($n_{H0}/n_{i0} = 0$) to the nominal value (indicated by vertical dashed lines in the frames of Fig. *5.*) and beyond. HYMAGYC observes two different modes, depending on the EP density range: for small values of n_{H0}/n_{i0} the most unstable (or less damped) mode is a mode radially located at $0.6 \lesssim s \lesssim 1$, in correspondence of the external throats within the toroidal gap ($\omega \approx -180$ kHz), which made the identification of this mode as a TAE. In a more internal radial region, centered radially around $s \approx 0.4$ and with frequency $\omega \lesssim -140$ kHZ, the mode already shown in the nominal value case, Fig. *4.* (left column) is observed, which is subdominant (larger damping or smaller growth rate) w.r.t. the TAE, in this range of EP density, and which we have already identified as a RSAE. For higher EP density values, $n_{H0}/n_{i0} \gtrsim 0.15$, the RSAE growth rate become dominant (i.e., it has the highest growth rate), and, eventually, is the only observable mode in the simulation. Similar results are observed by MEGA with close values to the ones observed by HYMAGYC, for both the frequencies and spatial location of the modes, but definitely smaller growth rate values. Also ORB5 observes the two different modes shown by HYMAGYC and MEGA, with the range of EP density where the RSAE dominates over the TAE being, in this case, above the nominal density case (i.e., for $n_{H0}/n_{i0} \gtrsim 0.4$). Moreover, growth rates observed by ORB5 are, generally speaking, larger that the ones observed by HYMAGYC and MEGA. It has to be noted that, when considering the slope of the growth rates obtained by the three codes for the TAE-like solution, and for the RSAE-like solution, they compare more favorably, suggesting that the differences observed (w.r.t. both the intensity of the growth rate and the relative dominance of one or the other mode) can be connected to differences between the damping retained by each code (e.g., continuum damping, resistive and viscous damping, as well as numerical damping), which result in different thresholds for unstable TAEs and RSAEs.

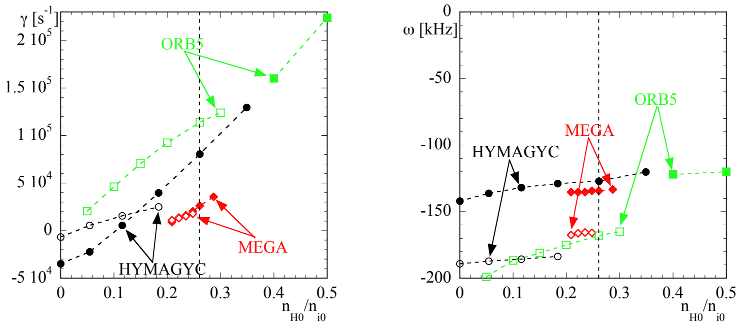

FIG. 5.: Energetic particle density scan for the AUG on-axis EP density profile: growth rates (left frame) and frequencies (right frame). Black circles refer to HYMAGYC results, red diamonds to MEGA, and green squares to ORB5, with closed symbols indicating RSAEs and open symbols to TAEs. The dashed black vertical lines refer to the nominal value of n_{H0}/n_{i0}.

Figure *6.* shows the results of the EP density scan for the peaked off-axis EP density profile. In this case, all the three codes observe, as the dominant mode, a TAE located close to the magnetic axis, with a frequency well within the toroidal gap, at $\omega \approx 150$ kHz.The radial profile of the Fourier components are very similar; growth rate obtained by ORB5 are larger that the ones obtained by HYMAGYC and MEGA; for this case, MEGA obtains slightly larger growth rates than HYMAGYC. Note that HYMAGYC, with a careful analysis of the frequency power spectra, is able to recognize also a sub-dominant, more external mode, characterized by a negative frequency $\omega \approx -200$ kHz, and located within the toroidal gap, at the radial position of the external throat, $s \approx 0.7$. Note that this mode is very similar to the one observed in the previous, peaked on-axis EP density profile case: indeed, the nominal EP density profiles for the peaked on-axis and the peaked off-axis EP density profiles almost overlap each other in the external, $s \gtrsim 0.5$, region of the discharge (see Fig. *2.*).

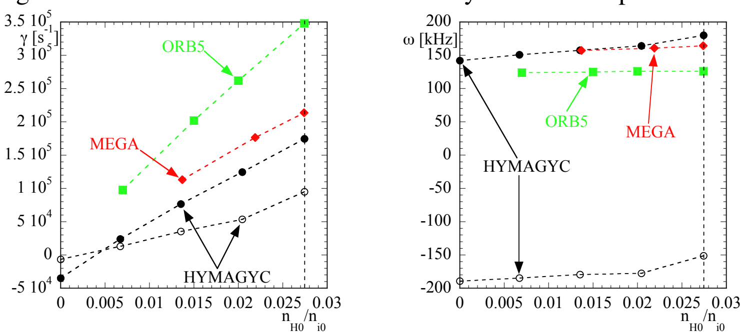

FIG. 6.: Energetic particle density scan for the AUG off-axis EP density profile: growth rates (left frame) and frequencies (right frame). Black circles refer to HYMAGYC results, red diamonds to MEGA, and green squares to ORB5, with closed symbols indicating core-localized TAEs and open symbols the external TAEs. The dashed black vertical lines refer to the nominal value of n_{H0}/n_{i0}.

4.3. ENERGETIC PARTICLE TEMPERATURE SCAN

In Figure *7.* the results of the simulations varying the EP temperature are shown, both for the peaked on-axis (top plots) and peaked off-axis (bottom plots) EP density profiles, while considering for each case, the nominal EP density values. For both the cases considered, the dependence of the growth rate and frequency is very similar, with the growth rate increasing weaker than linear with T_H (note, also, that for the peaked on-axis EP density profile case, the code ORB5 observes, at lower values of T_H ($T_H \lesssim 0.093$ keV), a TAE mode radially localized at the external throat of the toroidal gap (indicated in Fig. *7.* top figures, with open green squares), whereas HYMAGYC and MEGA observe a RSAE. On the other hand, for higher values of T_H ($T_H \gtrsim 0.093$ keV), and, thus, for stronger EP drive, also ORB5, as the other two codes, observes a RSAE as the dominant mode (indicated in Fig. 7. top figures, with filled green squares): indeed, the different nature of the mode observed by ORB5 at higher T_H is evident when noting the discontinuity in the frequency values (filled vs. open green squares in Fig. 7. top right figure).

Note also that, for the peaked off-axis EP density profile (Fig. 7. bottom figures), the code HYMAGYC is able to observe also the sub-dominant TAE mode (as in the EP density scan), located radially in the external TAE throat (open circle symbols), which behaves similar to the other dominant, internal TAE, as T_H is varied. As a general consideration, the dependence of the growth rate, w.r.t. the EP temperature, is similar among the three codes, ORB5 showing typically a stronger net growth rate than the two hybrid codes.

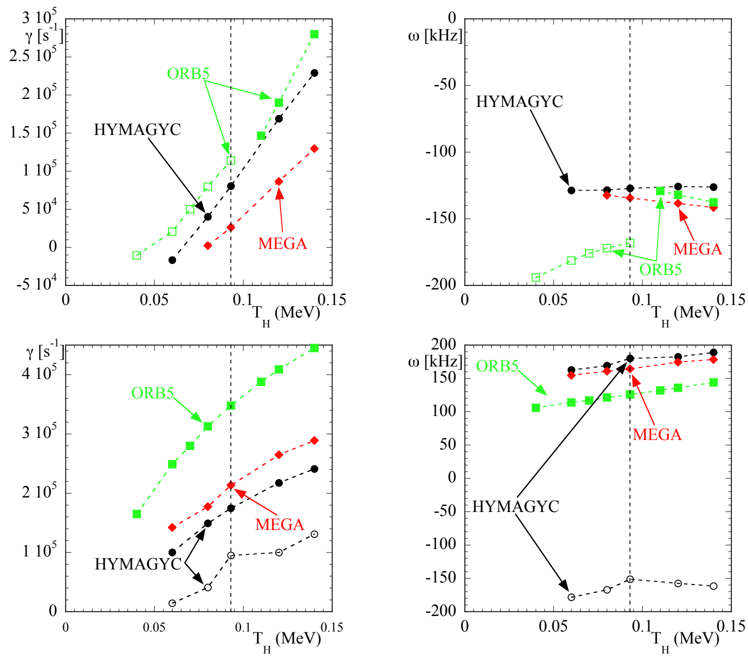

FIG. 7.: Growth rates (left column) and frequencies (right column) vs. T_H for the on-axis (top row) and off-axis (bottom row) EP density profiles. Black circles refer to HYMAGYC results, red diamonds to MEGA, and green squares to ORB5. The dashed black vertical lines refer to the nominal value of T_{H0}.

5. CONCLUSIONS

In this paper the two hybrid MHD-gyrokinetic codes HYMAGYC and MEGA and the full gyrokinetic code ORB5 have been benchmarked, in the linear regime, by studying the EP driven Alfvénic modes in a realistic equilibrium, namely, the AUG-NLED test case. Purely MHD spectra of oscillation have been first compared, and then the linear stability for both on-axis and off-axis peaked EP density profiles equilibria have been considered. Some differences have been observed among the codes at the nominal values of the benchmark, in particular fo the on-axis case; nevertheless, when considering EP density and temperature scans, a fairly good agreement among the three codes is, indeed, obtained.

Acknowledgment: This work has been carried out within the framework of the EUROfusion Consortium and has received funding from the Euratom research and training programme 2014-2018 and 2019-2020 under grant agreement No 633053. The views and opinions expressed herein do not necessarily reflect those of the European Commission. The computing resources and the related technical support used for this work have been provided by EUROfusion and the EUROfusion High Performance Computer (Marconi-Fusion).

References

[1] MET Enabling Research Project, `https://www.afs.enea.it/zonca/METproject/index.html`

[2] Aymar R. et al. 1997, FEC 1996, IAEA, Vol. 1, p.3

[3] JT-60SA Research Plan: `http://www.jt60sa.org/pdfs/JT-60SA_Res_Plan.pdf`

[4] DTT Interim Design Report, `https://www.dtt-project.enea.it/downloads/DTT_IDR_2019_WEB.pdf`

[5] G. Fogaccia, G. Vlad, S. Briguglio, Nucl. Fusion 56 (2016) 112004

[6] Y. Todo, Phys. Plasmas 13, 082503 (2006)

[7] E. Lanti et al., Computer Physics Communications 251:107072, 2020

[8] Ph. Lauber, “The NLED reference case”, ASDEX Upgrade Ringberg Seminar (2016), (Ph. Lauber et al., NLED-AUG reference case, `http://www2.ipp.mpg.de/~pwl/NLED_AUG/data.html`)

[9] Ph. Lauber et al, EX1/1 Proc. 27th IAEA FEC (2018)

[10] Lütjens H., Bondeson A. and Sauter O. 1996 Comput. Phys. Commun. 97 219–60

[11] F. Imbeaux et al. *Comp. Phys. Comm.* 181(6):987-998, 2010

[12] F. Imbeaux et al., 2015 Nucl. Fusion 55 123006

[13] A. Bondeson, G. Vlad, and H. Lütjens. In *IAEA Technical Committee Meeting on Advances in Simulations and Modelling of Thermonuclear Plasmas, Montreal, 1992*, page 306, Vienna, Austria, 1993. International Atomic Energy Agency.

[14] G. Vlad, F. Zonca, and S. Briguglio. *Rivista del Nuovo Cimento*, 22(7):1-97, 1999.

[15] A. Bondeson and G.Y. Fu. *Comput. Phys. Comm.* 66:167-176, 1991.

[16] E.A. Frieman and L. Chen, *Phys. Fluids*, 25 502, 1982.

[17] Park W. et al., *Phys. Fluids* B ,4 2033, 1992.

[18] R. D. Hazeltine and J. D. Meiss, “Plasma Confinement” (Addison-Wesley, Redwood City) p.222 (1992).

[19] N. Tronko, A. Bottino, and E. Sonnendrücker. Physics of Plasmas, 23(8):082505, 2016.

[20] N. Tronko, A. Bottino, C. Chandre, and E Sonnendrüecker. Plasma Physics and Controlled Fusion, 59(6):064008, 2017.

[21] Jolliet S. et al., 2007 Comput. Phys. 177 409

[22] A. Mishchenko, et al.. Computer Physics Communications, 238:194 – 202, 2019.

[23] O. Sauter and S. Yu. Medvedev, Computer Physics Communications 184 (2013) 293

[24] Falessi, M.V., Carlevaro, N., Fusco, V., Vlad, G. and Zonca, F., Phys. Plasmas, vol. 26, issue 8, 2019, 082502

[25] Falessi, M.V., Carlevaro, N., Fusco, V., Giovannozzi, E., Lauber, Ph., Vlad, G. and Zonca, F., J. Plasma Phys. (2020), vol. 86, 845860501

[26] Chen L, White RB and Rosenbluth MN 1984 *Phys. Rev. Lett.* **52** 1122–1125